Electronic Supplementary Material (ESI) for Faraday Discussions.

Supporting information for:

MOF Matrix Isolation: Cooperative Conformational Mobility Enables Reliable Single Crystal Transformations

Ricardo A. Peralta,[a] Michael T. Huxley,[a] Rosemary J. Young,[a] Oliver M Linder-Patton,[a] Jack D. Evans,[b] Christian J. Doonan[a] and Christopher J. Sumby*[a]

a. Department of Chemistry and Centre for Advanced Nanomaterials, The University of Adelaide, Adelaide, Australia. Email: christopher.sumby@adelaide.edu.au

b. Department of Inorganic Chemistry, Technische Universität Dresden, Bergstraße 66, 01062 Dresden, Germany.

SI 1.0 Monitoring solvent exchange within MnMOF-1

Herein, X-ray crystallography was employed to study the effects of solvation in **MnMOF-1**, in particular the effect of solvent on the conformation of the free pyrazole sites within the material. Although it is clear that solvent exchange induces structural transformations (e.g. 'syn' and 'anti' conformation) over the course of 24 hr (5 washes), it is not clear how long it takes to fully exchange the solvent within the MOF pores and whether the solvent is fully exchanged within the cavities of framework. To investigate these factors, key solvent exchange processes from DMF to acetone, acetone to diethyl ether, acetone to DCM, acetone to THF and acetone to *p*-xylene were monitored via NMR spectroscopy. For example, **MnMOF-1-as** was exchanged with fresh acetone a number of times over the course of 90 minutes, and after each exchange a portion of the MOF crystals was removed, dried briefly under a flow of Ar and digested in D_6-DMSO/DCl for analysis by NMR spectroscopy. This allowed the proportion of DMF and acetone to be determined, revealing that solvent exchange takes place rapidly and is complete within three solvent exchanges.

In the other solvent exchange processes the same method was applied. The trend was similar to the first experiment described above; the solvent exchange occurs rapidly and is complete within the first three exchanges. These experiments verify that the solvent exchange procedure used to prepare samples for crystallographic studies successfully substitute the solvent within the MOF pores.

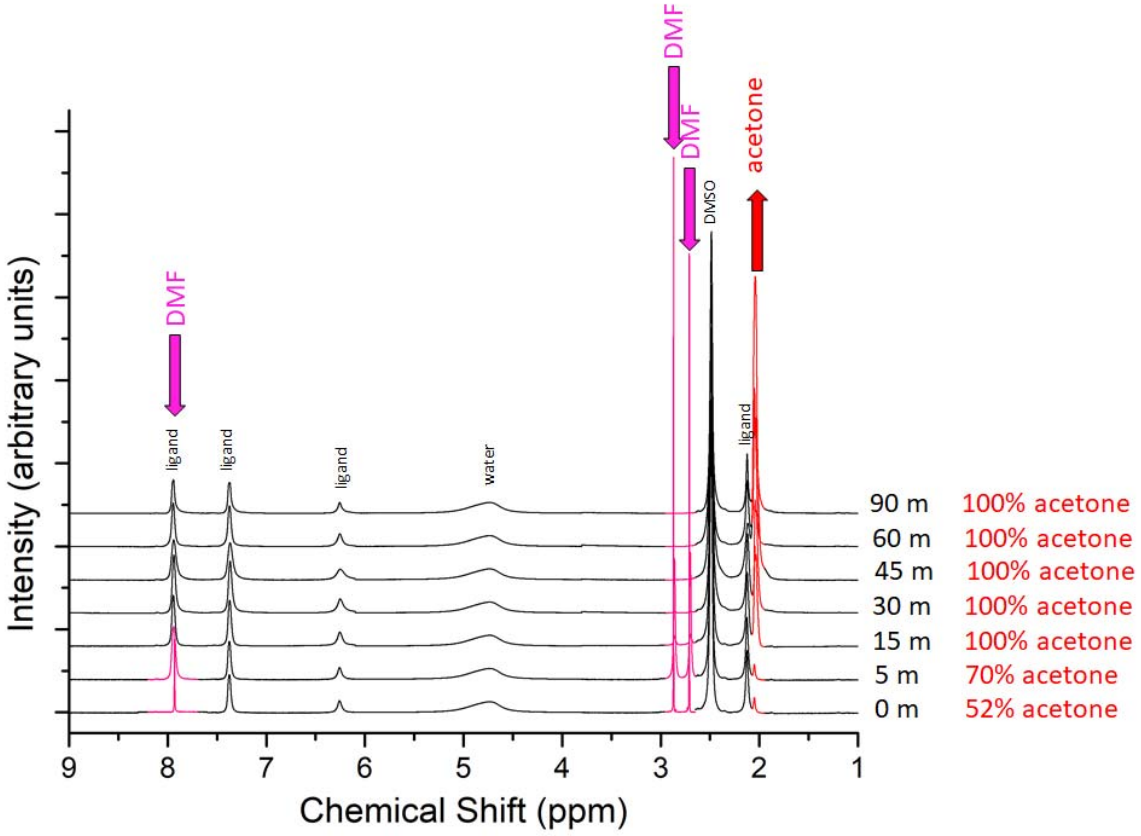

Figure S1.1. Sample **MnMOF-1-DMF** was washed recurrently 6 times with acetone during the course of 90 minutes, each time the sample was allowed to soak for the specified time before the next solvent exchange was performed. After the solvent was changed, a portion of the MOF material was dried briefly under Ar flow and analysed by NMR (digested in D_6-DMSO/DCl) to quantify the proportions of DMF and acetone present within the MOF pores

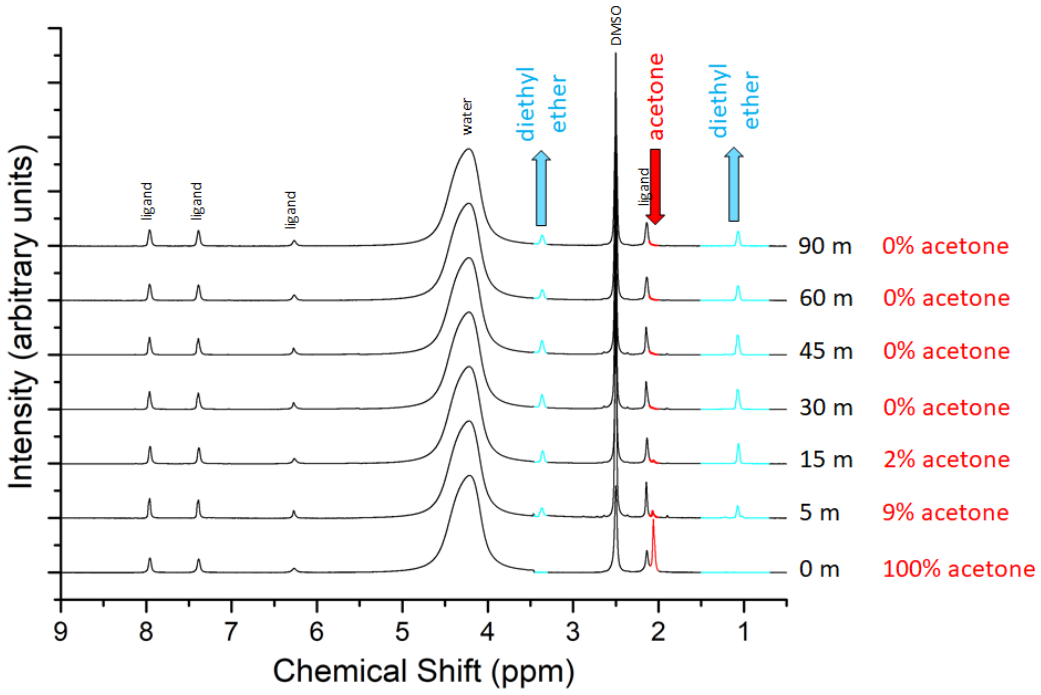

Figure S1.2. Sample **MnMOF-1-ace** was washed recurrently 6 times with diethyl ether during the course of 90 minutes, each time the sample was allowed to soak certain time before adding new solvent. After the solvent was changed, a portion of the material was dried softly under Ar flow and analysed by NMR (digested in D_6-DMSO/DCl) to quantify the amount of acetone remained in each washed.

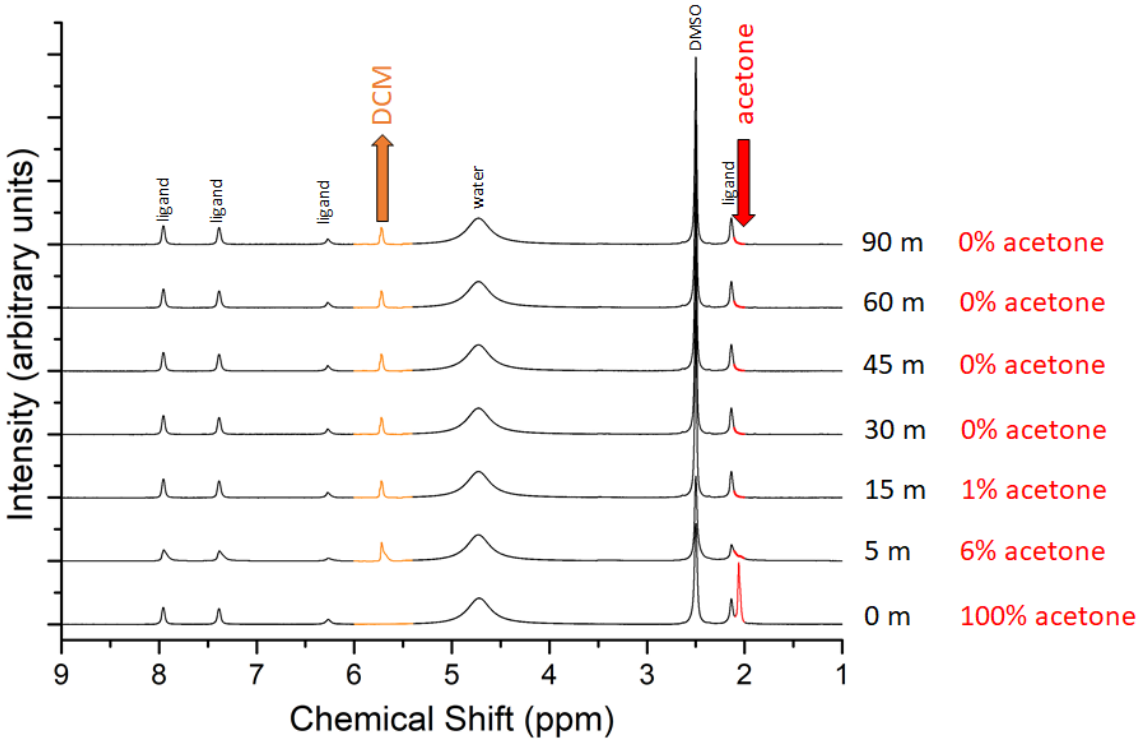

Figure S1.3. Sample **MnMOF-1-ace** was washed recurrently 6 times with DCM during the course of 90 minutes, each time the sample was allowed to soak certain time before adding new solvent. After the solvent was changed, a portion of the material was dried softly under Ar flow and analysed by NMR (digested in D_6-DMSO/DCl) to quantify the amount of acetone remained in each washed.

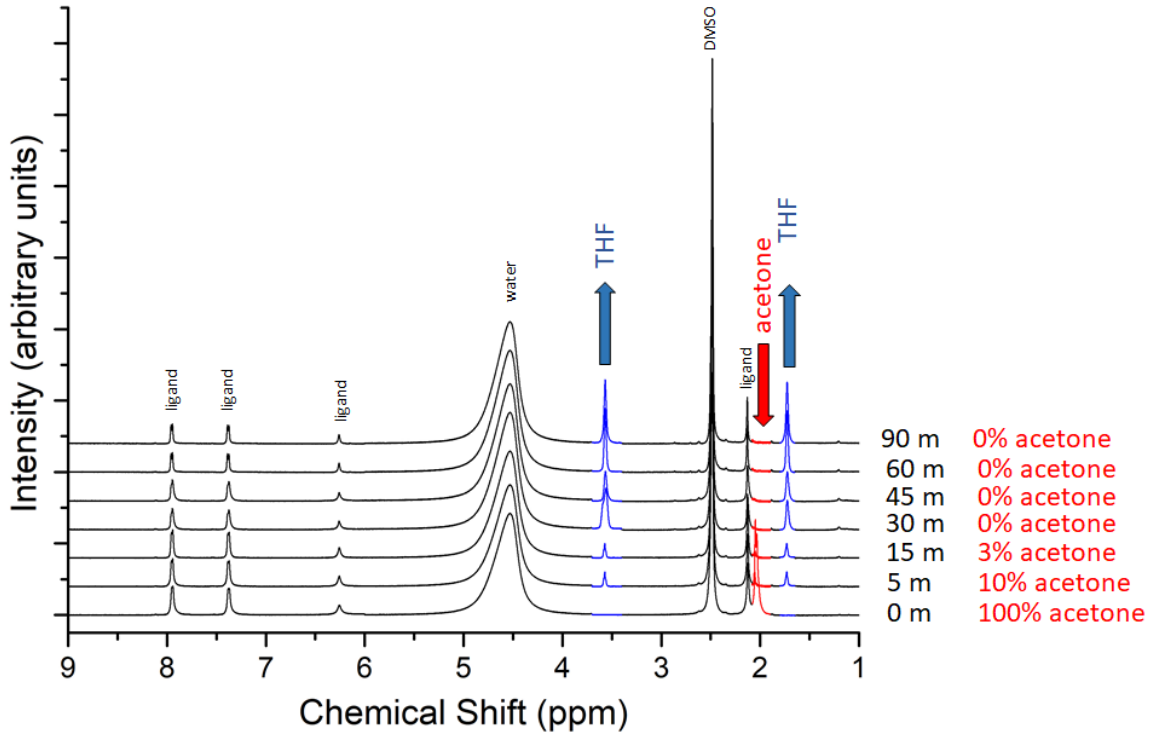

Figure S1.4. Sample **MnMOF-1-ace** was washed recurrently 6 times with THF during the course of 90 minutes, each time the sample was allowed to soak certain time before adding new solvent. After the solvent was changed, a portion of the material was dried softly under Ar flow and analysed by NMR (digested in D_6-DMSO/DCl) to quantify the amount of acetone remained in each washed.

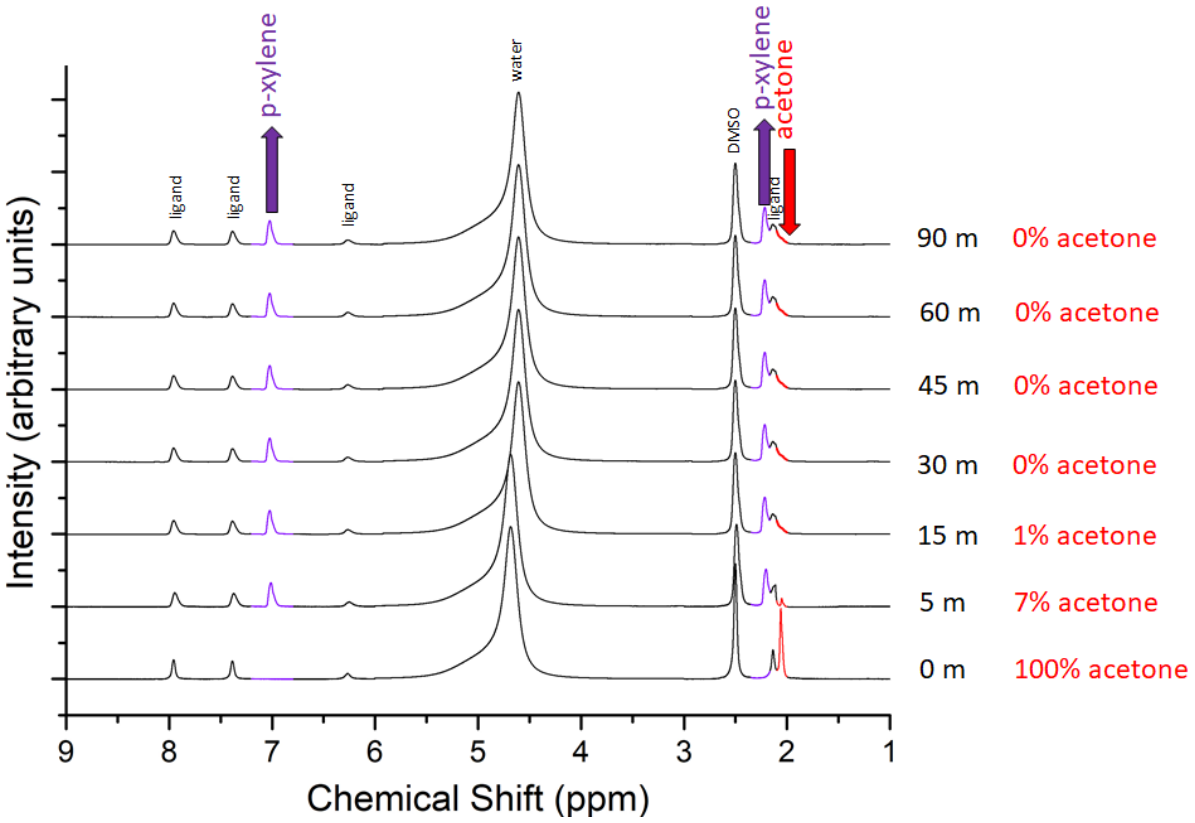

Figure S1.5. Sample **MnMOF-1-ace** was washed recurrently 6 times with *p*-xylene during the course of 90 minutes, each time the sample was allowed to soak for the specified time before adding new solvent. After the solvent was changed, a portion of the material was dried softly under Ar flow and analysed by NMR (digested in D_6-DMSO/DCl) to quantify the amount of acetone remained in each washed.

SI 2.0 IR spectroscopy following reaction between solvated MnMOF-1 samples and $[Rh(CO)_2Cl]_2$

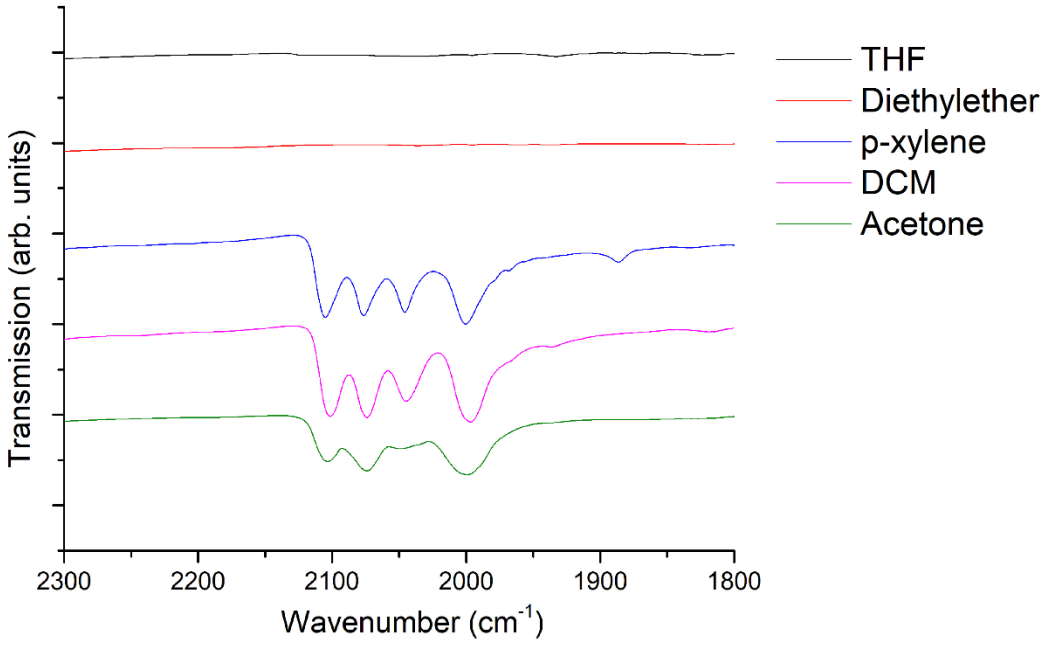

Figure S2.0. IR spectra of **MnMOF-1** after reaction with $[Rh(CO)_2Cl]_2$ in different solvents. The presence of strong CO stretching bands near 2000 cm^{-1} confirms the successful metalation of **MnMOF-1** to form **MnMOF-1**·$[Rh(CO)_2][Rh(CO)_2Cl_2]$ in *p*-xylene, DCM and acetone. The same reaction performed in THF or diethylether does not result in metalation, as evidenced by the absence of CO stretching bands in the IR spectrum.

SI 3.0 Powder X-ray diffractograms of each sample

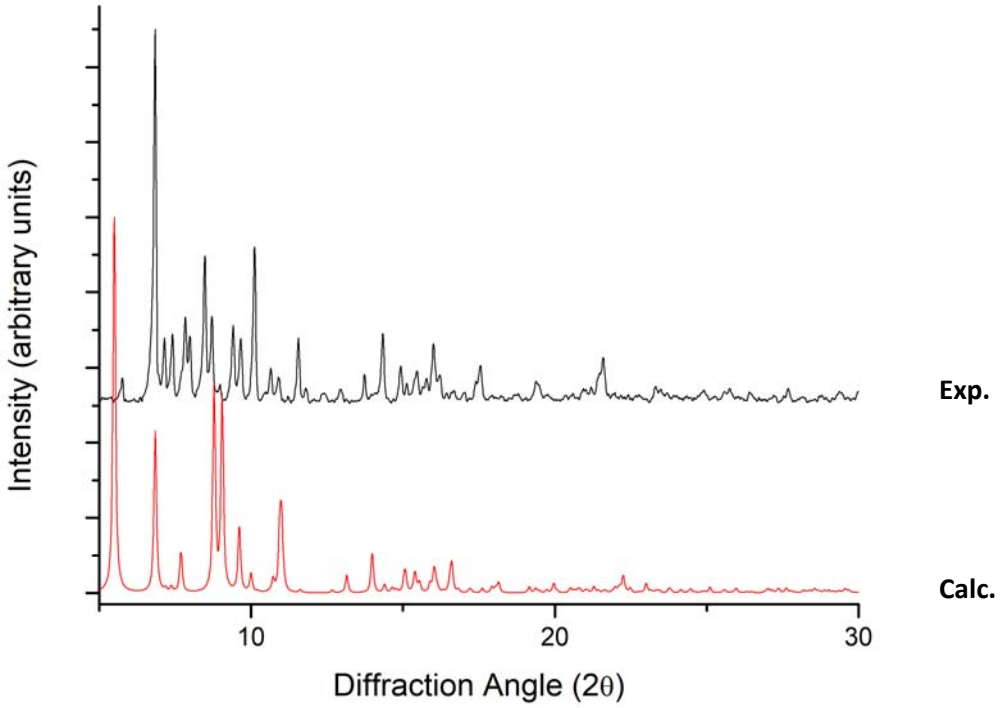

Figure S3.1. PXRD pattern obtained for **MnMOF-1-MeOH** (exp, dried) and simulated PXRD pattern generated from the single crystal X-ray structure (calc). The experimental PXRD pattern obtained here shows features consistent with structural contraction following desolvation.

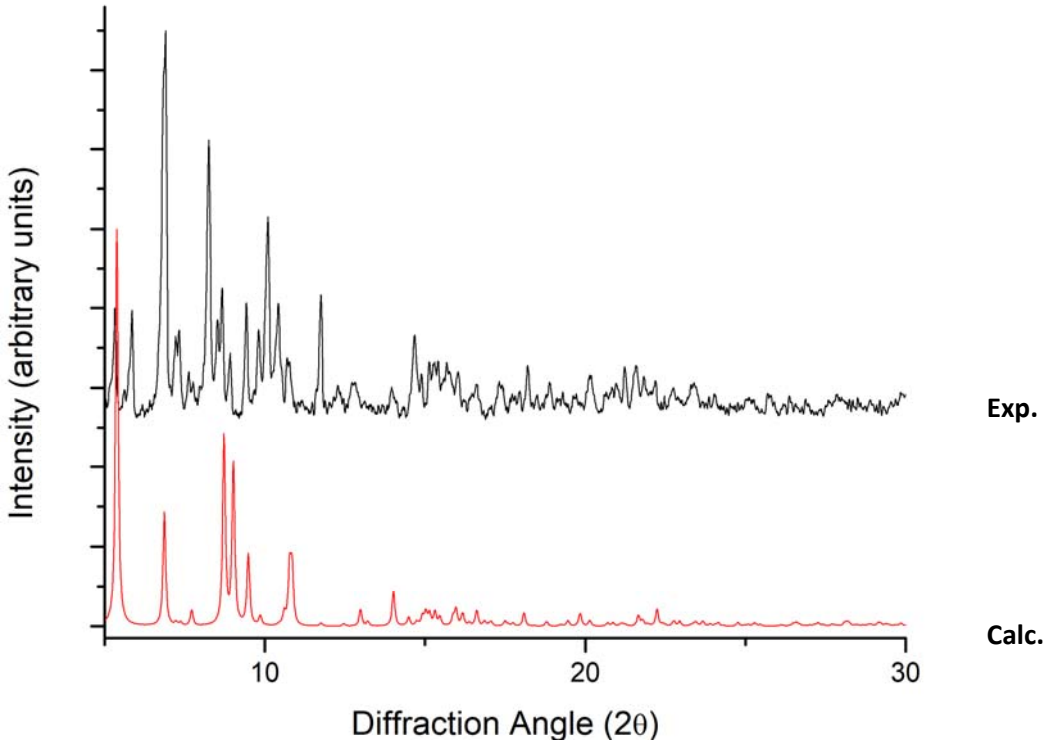

Figure S3.2. PXRD pattern obtained for **MnMOF-1-EtOH** (exp, dried) and simulated PXRD pattern generated from the single crystal X-ray structure (calc). The experimental PXRD pattern obtained here shows features consistent with structural contraction following desolvation.

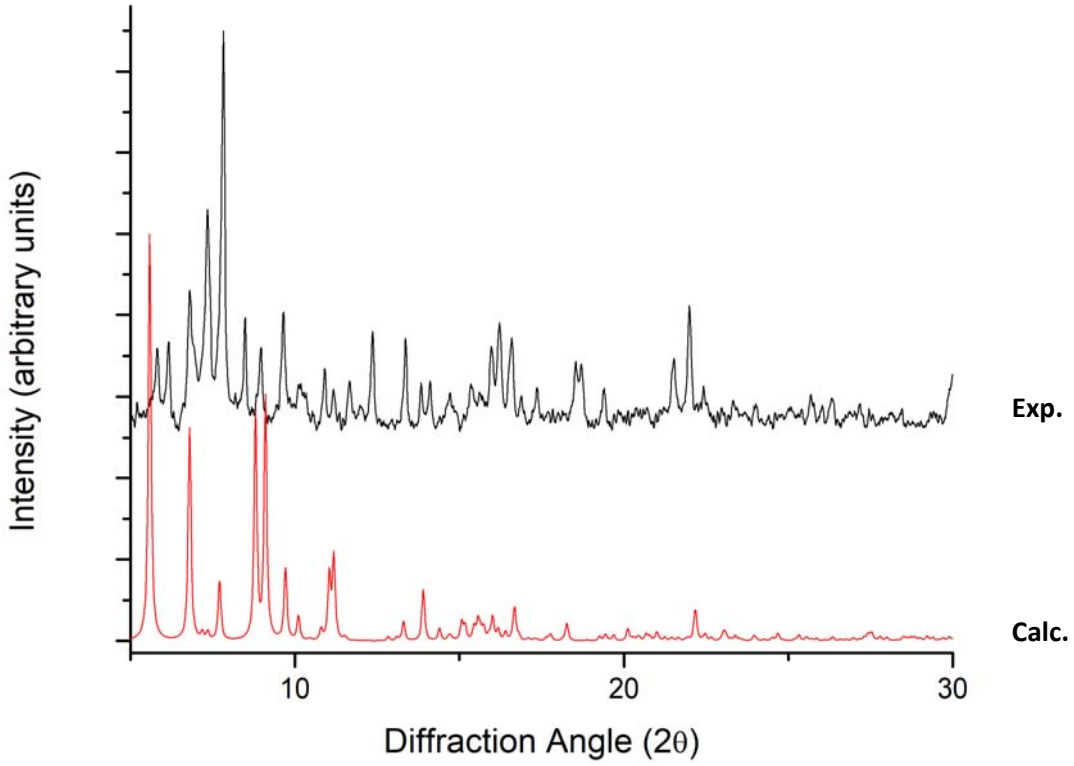

Figure S3.3. PXRD pattern obtained for **MnMOF-1-ace** (exp, dried) and simulated PXRD pattern generated from the single crystal X-ray structure (calc). The experimental PXRD pattern obtained here shows features consistent with structural contraction following desolvation.

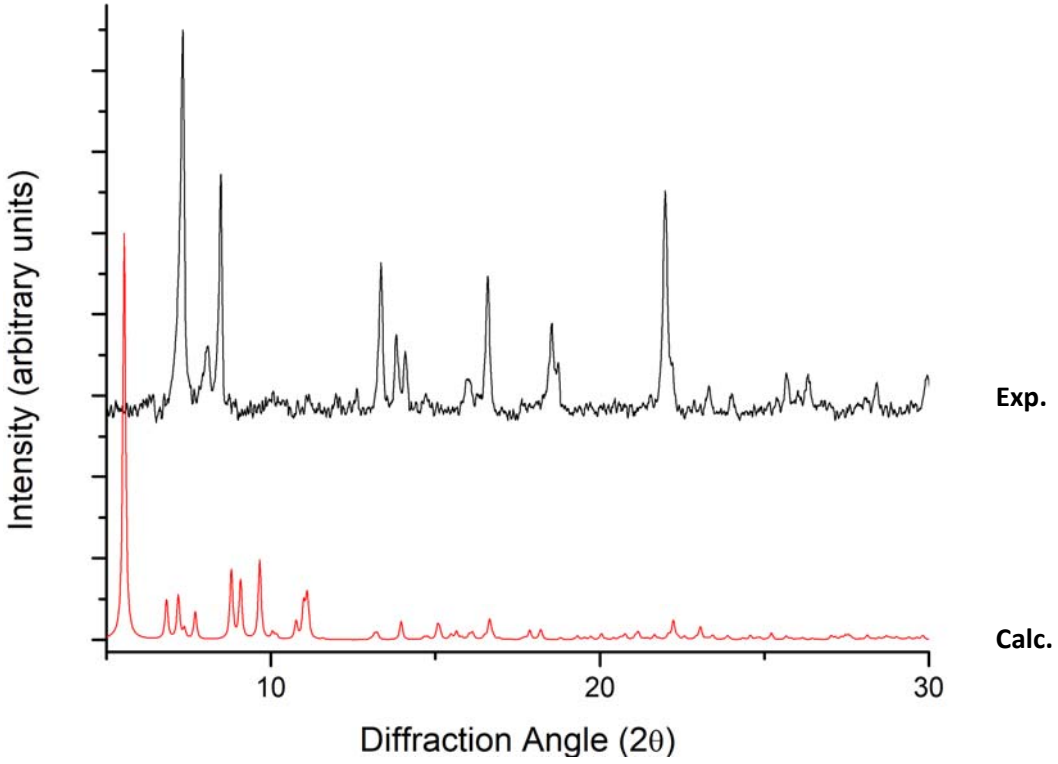

Figure S3.4. PXRD pattern obtained for **MnMOF-1-DCM** (exp, dried) and simulated PXRD pattern generated from the single crystal X-ray structure (calc). The experimental PXRD pattern obtained here shows features consistent with structural contraction following desolvation.

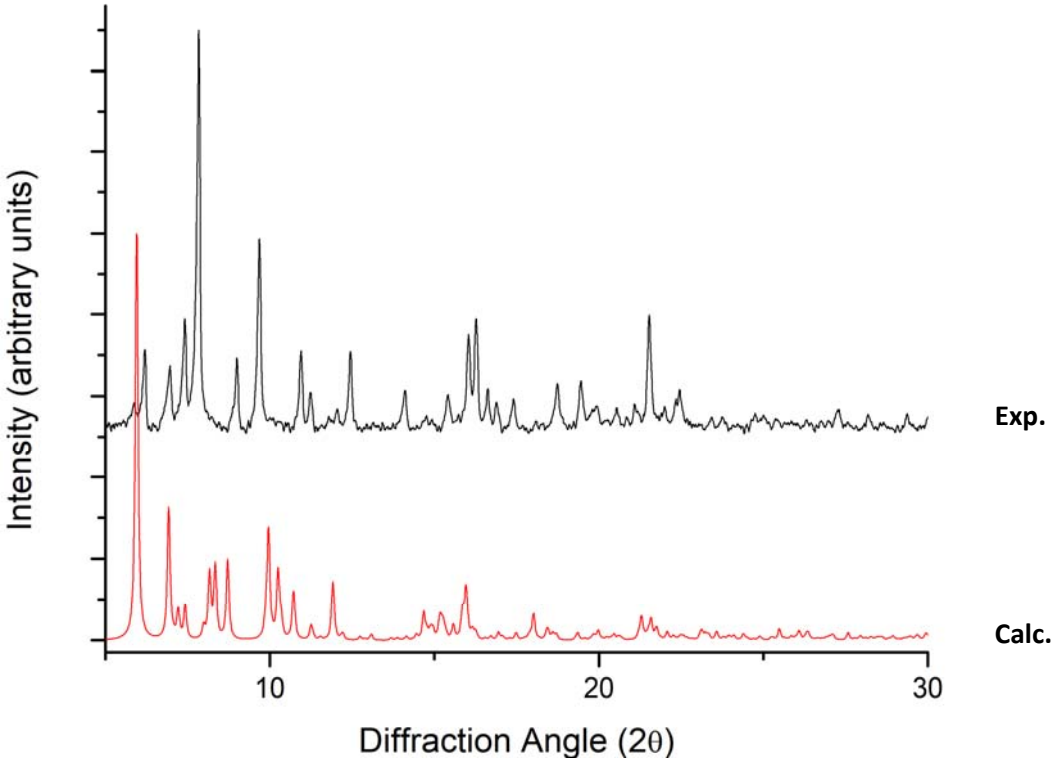

Figure S3.5. PXRD pattern obtained for **MnMOF-1-DEE** (exp, dried) and simulated PXRD pattern generated from the single crystal X-ray structure (calc). The experimental PXRD pattern obtained here shows features consistent with structural contraction following desolvation.

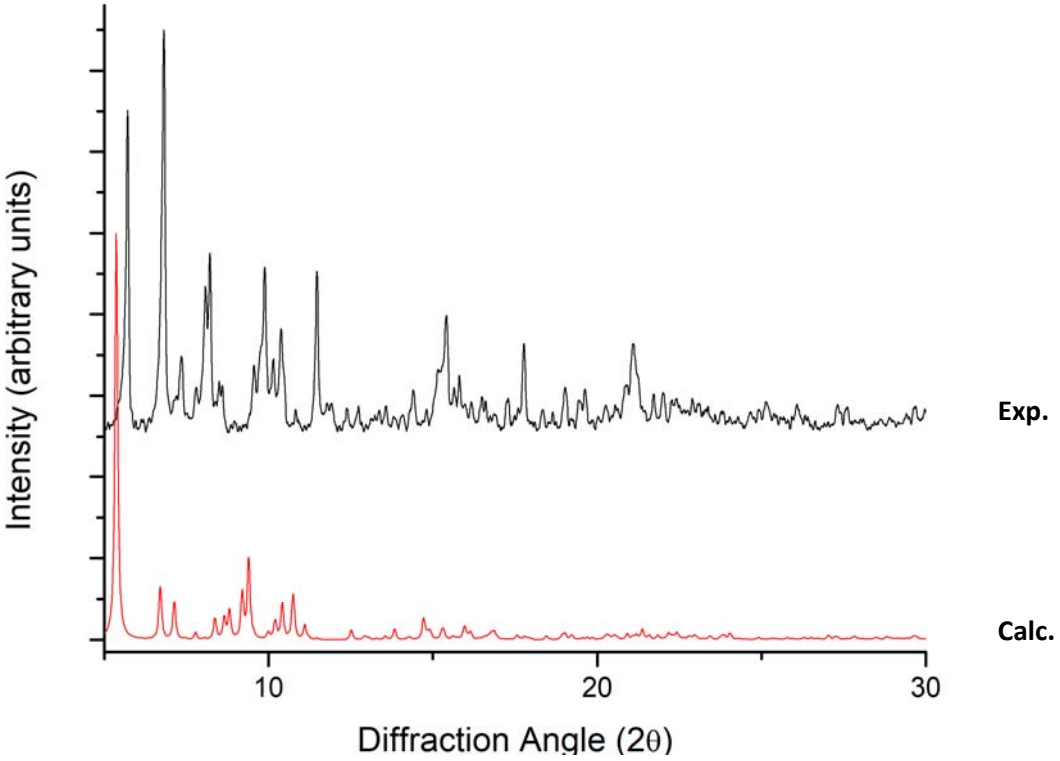

Figure S3.6. PXRD pattern obtained for **MnMOF-1-THF** (exp, dried) and simulated PXRD pattern generated from the single crystal X-ray structure (calc). The experimental PXRD pattern obtained here shows features consistent with structural contraction following desolvation.

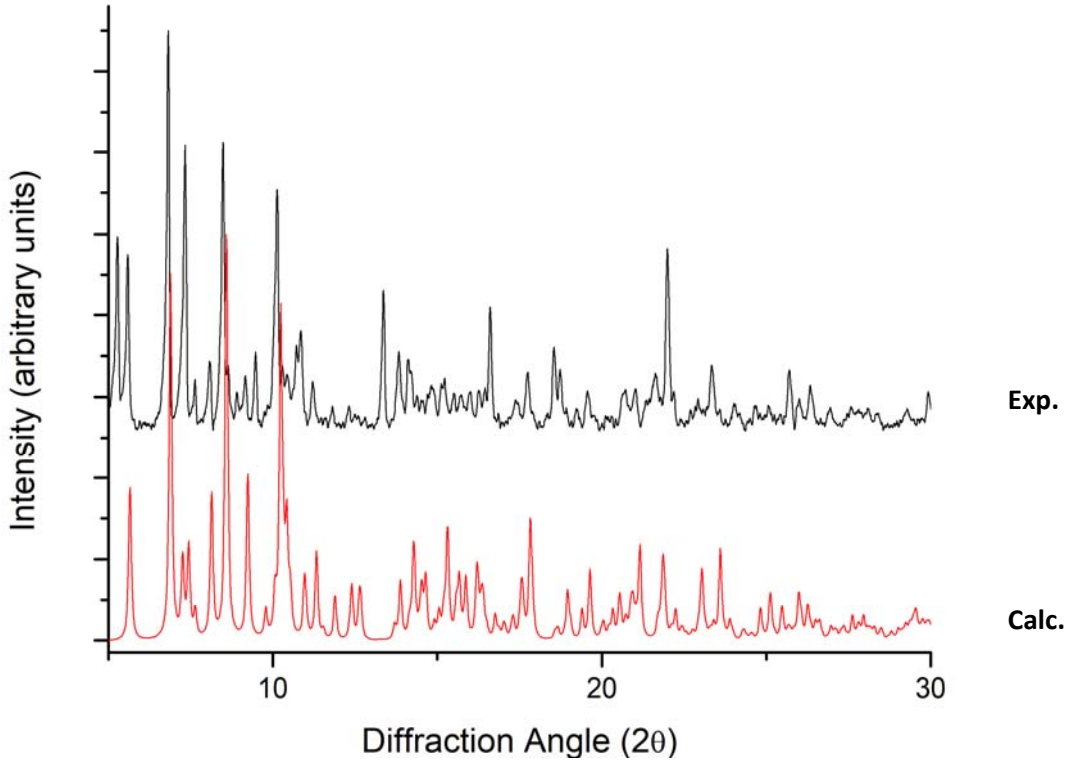

Figure S3.7. PXRD pattern obtained for **MnMOF-1-*p-xylene*** (exp, dried) and simulated PXRD pattern generated from the single crystal X-ray structure (calc).

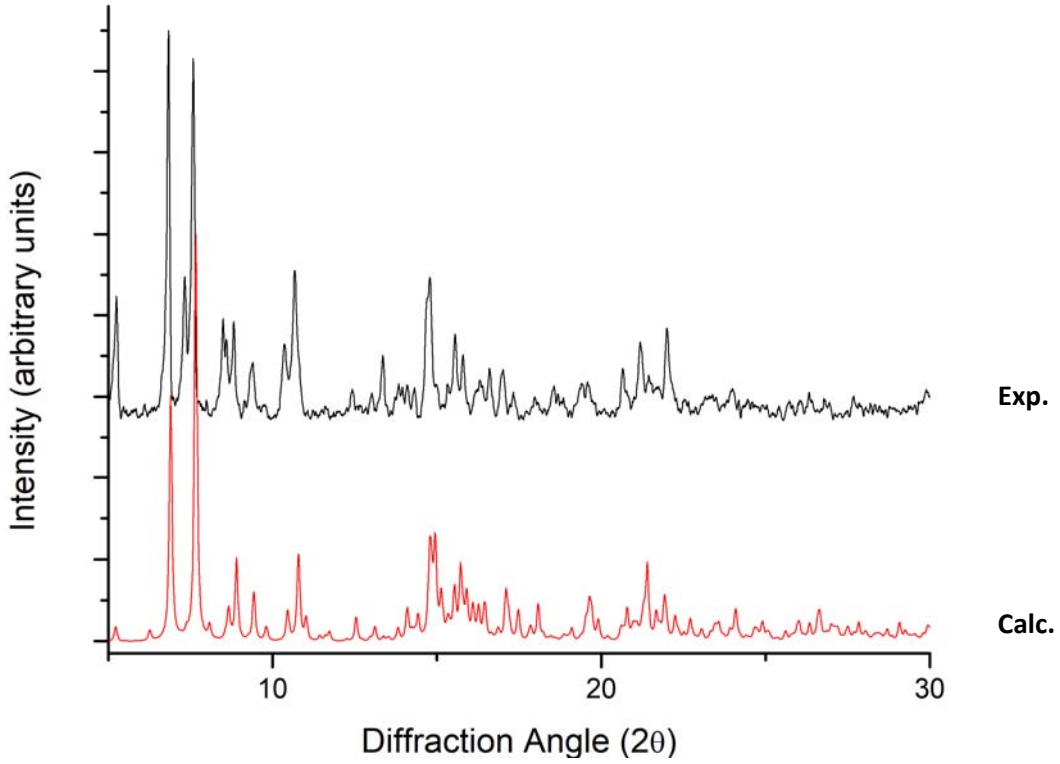

Figure S3.8. PXRD pattern obtained for **MnMOF-1**·$[Rh(CO)_2][RhCl_2(CO)_2]$ prepared in *p*-xylene (exp, dried) and simulated PXRD pattern generated from the single crystal X-ray structure (calc).

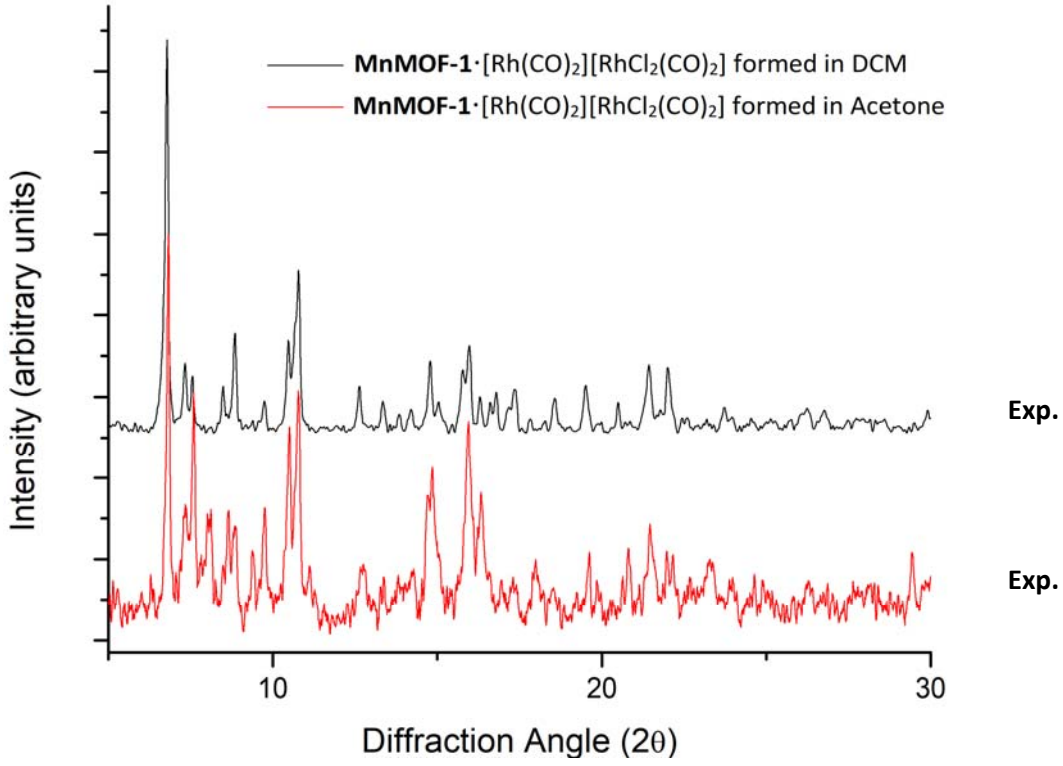

Figure S3.9. PXRD pattern obtained for **MnMOF-1**·$[Rh(CO)_2][RhCl_2(CO)_2]$ prepared in DCM (exp) and acetone (exp).

SI 4.0 Structure refinement details and tables of crystallographic parameters for the structures

Specific refinement details

MnMOF-1(MeOH). The structure possessed solvent accessible pores and in order to subtract the contribution from the disordered solvent, the SQUEEZE routine available in Platon[1] was applied to the data. Refinement against the new HKL file gave an improvement in R_1, wR_2 and *GooF*. The disorder of the bispyrazole site was modelled through the use of DFIX, EADP, EXYZ, FLAT and SIMU restraints.

MnMOF-1(p-xylene). The MOF structure and the solvate *p*-xylene were well ordered in this structure. A FLAT restraint was used to help the refinement of a xylene molecule.

MnMOF-1(DEE). The structure possessed solvent accessible pores and in order to subtract the contribution from the disordered solvent, the SQUEEZE routine available in Platon[1] was applied to the data. Refinement against the new HKL file gave an improvement in R_1, wR_2 and *GooF*.

MnMOF-1(EtOH). Like the methanol solvate, the structure possessed solvent accessible pores and in order to subtract the contribution from the disordered solvent, the SQUEEZE routine available in Platon[1] was applied to the data. Refinement against the new HKL file gave an improvement in R_1, wR_2 and *GooF*. The disorder of the bispyrazole site was modelled through the use of DFIX, EADP, EXYZ, FLAT and SIMU restraints.

MnMOF-1(DCM). Like the methanol solvate, the structure possessed solvent accessible pores and in order to subtract the contribution from the disordered solvent, the SQUEEZE routine available in Platon[1] was applied to the data. Refinement against the new HKL file gave an improvement in R_1, wR_2 and *GooF*. The disorder of the bispyrazole site was modelled through the use of DFIX, EADP, EXYZ, FLAT and SIMU restraints.

MnMOF-1(acetone). Like the methanol solvate, the structure possessed solvent accessible pores and in order to subtract the contribution from the disordered solvent, the SQUEEZE routine available in Platon[1] was applied to the data. Refinement against the new HKL file gave an improvement in R_1, wR_2 and *GooF*. The disorder of the bispyrazole site was modelled through the use of DFIX, EADP, EXYZ, FLAT and SIMU restraints.

MnMOF-1(THF). The structure possessed solvent accessible pores and in order to subtract the contribution from the disordered solvent, the SQUEEZE routine available in Platon[1] was applied to the data. Refinement against the new HKL file gave an improvement in R_1, wR_2 and *GooF*. DFIX restraints were used to aid the refinement of THF molecules located in the structure.

1. Spek, A. L. PLATON SQUEEZE: a tool for the calculation of the disordered solvent contribution to the calculated structure factors. *Acta. Crystallogr. C Struct. Chem*. **2015,** 71, 9-18.

Table S4.1. X-ray experimental data for **MnMOF-1(MeOH)**, **MnMOF-1(p-xylene)**, and **MnMOF-1(DEE)**.

Compound	**MnMOF-1(MeOH)**	**MnMOF-1(p-xylene)**	**MnMOF-1(DEE)**
CCDC #	1977797	1977798	1977799
Empirical formula	$C_{90}H_{126}N_{12}O_{27}Mn_3$	$C_{105}H_{103.5}N_{12}O_{12}Mn_3$	$C_{97}H_{126}N_{12}O_{18}Mn_3$
Formula weight	1972.84	1890.31	1912.91
Crystal system	monoclinic	triclinic	triclinic
Space group	$P2_1/m$	P-1	P-1
a/Å	12.323(3)	12.276(3)	12.364(3)
b/Å	32.145(6)	12.869(3)	12.947(3)
c/Å	12.931(3)	31.586(6)	30.366(6)
α/°	90	93.98(3)	99.40(3)
β/°	93.58(3)	97.43(3)	97.35(3)
γ/°	90	92.02(3)	91.57(3)
Volume/Å^3	5112.3(18)	4931.1(18)	4750.4(17)
Z	2	2	2
ρ_{calc}g/cm^3	1.282	1.273	1.337
μ/mm^{-1}	0.442	0.444	0.466
F(000)	2082.0	1977.0	2022.0
Crystal size/mm^3	0.65 × 0.25 × 0.07	0.6 × 0.26 × 0.06	0.7 × 0.3 × 0.08
2Θ range for data collection/°	2.534 to 58.376	1.304 to 58.198	1.372 to 58.324
Reflections collected	64425	50428	53314
Independent reflections	10099 [R_{int} = 0.0389, R_{sigma} = 0.0224]	17416 [R_{int} = 0.0744, R_{sigma} = 0.0870]	17030 [R_{int} = 0.0398, R_{sigma} = 0.0443]
Data/restraints/parameters	10099/148/577	17416/1/1210	17030/0/1028
Goodness-of-fit on F^2	1.090	1.663	2.437
Final R indexes [I>=2σ (I)]	R_1 = 0.0602, wR_2 = 0.1927	R_1 = 0.1480, wR_2 = 0.4430	R_1 = 0.2135, wR_2 = 0.5779
Final R indexes [all data]	R_1 = 0.0671, wR_2 = 0.1983	R_1 = 0.1959, wR_2 = 0.4652	R_1 = 0.2500, wR_2 = 0.5982
Largest diff. peak/hole / e Å^{-3}	0.42/-0.56	2.06/-1.03	1.62/-1.17

Table S4.1 (cont'd). X-ray experimental data for **MnMOF-1(EtOH)**, **MnMOF-1**[$Rh(CO)_2$][$RhCl_2(CO)_2$](p-xylene), and **MnMOF-1(DCM)**.

Compound	**MnMOF-1(EtOH)**	**MnMOF-1**[$Rh(CO)_2$][$RhCl_2(CO)_2$](p-xylene)	**MnMOF-1(DCM)**
CCDC #	1977800	1977801	1977802
Empirical formula	$C_{93}H_{120}N_{12}O_{21}Mn_3$	$C_{111}H_{106}N_{12}O_{16}Mn_3Rh_2Cl_2$	$C_{84}H_{84}N_{12}O_{12}Mn_3Cl_{18}$
Formula weight	1906.82	2305.61	2256.55
Crystal system	monoclinic	monoclinic	monoclinic
Space group	$P2_1/m$	$P2_1/c$	$P2_1/m$
a/Å	12.274(3)	12.339(3)	12.313(3)
b/Å	32.826(7)	33.798(7)	31.877(6)
c/Å	12.930(3)	25.762(5)	12.954(3)
α/°	90	90	90
β/°	95.51(3)	96.10(3)	92.93(3)
γ/°	90	90	90
Volume/$Å^3$	5185.5(18)	10683(4)	5077.8(18)
Z	2	4	2
$\rho_{calc}g/cm^3$	1.221	1.434	1.476
μ/mm^{-1}	0.429	0.767	0.902
F(000)	2010.0	4732.0	2298.0
Crystal size/mm^3	0.7 × 0.4 × 0.09	0.66 × 0.32 × 0.06	0.8 × 0.35 × 0.1
2Θ range for data collection/°	3.164 to 58.438	1.996 to 58.298	2.556 to 63.734
Reflections collected	67817	136906	92980
Independent reflections	10346 [R_{int} = 0.0258, R_{sigma} = 0.0156]	22874 [R_{int} = 0.0904, R_{sigma} = 0.0611]	14475 [R_{int} = 0.0927, R_{sigma} = 0.0681]
Data/restraints/parameters	10346/160/577	22874/0/1335	14475/151/604
Goodness-of-fit on F^2	1.073	1.033	1.090
Final R indexes [I>=2σ (I)]	R_1 = 0.0480, wR_2 = 0.1433	R_1 = 0.1033, wR_2 = 0.2994	R_1 = 0.1010, wR_2 = 0.2925
Final R indexes [all data]	R_1 = 0.0522, wR_2 = 0.1467	R_1 = 0.1554, wR_2 = 0.3403	R_1 = 0.1410, wR_2 = 0.3127
Largest diff. peak/hole / e $Å^{-3}$	0.38/-0.64	2.12/-1.36	0.91/-1.08

Table S4.1 (cont'd). X-ray experimental data for **MnMOF-1(acetone)** and **MnMOF-1(THF)**.

Compound	**MnMOF-1(acetone)**	**MnMOF-1(THF)**
CCDC #	1977803	1977804
Empirical formula	$C_{97.5}H_{111}N_{12}O_{19.5}Mn_3$	$C_{111}H_{138}Mn_3N_{12}O_{21}$
Formula weight	1927.80	2141.15
Crystal system	monoclinic	triclinic
Space group	$P2_1/m$	P-1
a/Å	12.307(3)	12.457(3)
b/Å	31.637(6)	13.242(3)
c/Å	13.006(3)	33.037(7)
α/°	90	86.69(3)
β/°	92.10(3)	86.08(3)
γ/°	90	85.22(3)
Volume/Å^3	5060.6(18)	5411(2)
Z	2	2
ρ_{calc}g/cm^3	1.265	1.314
μ/mm^{-1}	0.439	0.419
F(000)	2022.0	2262.0
Crystal size/mm^3	0.09 × 0.04 × 0.01	0.7 × 0.36 × 0.08
2Θ range for data collection/°	3.134 to 63.434	1.238 to 65.206
Reflections collected	92993	76155
Independent reflections	14274 [R_{int} = 0.0939, R_{sigma} = 0.0599]	27046 [R_{int} = 0.1176, R_{sigma} = 0.1696]
Data/restraints/parameters	14274/152/577	27046/39/1014
Goodness-of-fit on F^2	1.044	1.128
Final R indexes [I>=2σ (I)]	R_1 = 0.0726, wR_2 = 0.2023	R_1 = 0.2041, wR_2 = 0.4668
Final R indexes [all data]	R_1 = 0.1086, wR_2 = 0.2198	R_1 = 0.2796, wR_2 = 0.5044
Largest diff. peak/hole / e Å^{-3}	0.98/-1.13	1.37/-1.33

SI 5.0 Thermal ellipsoid plots for all structures at the 50% probability level

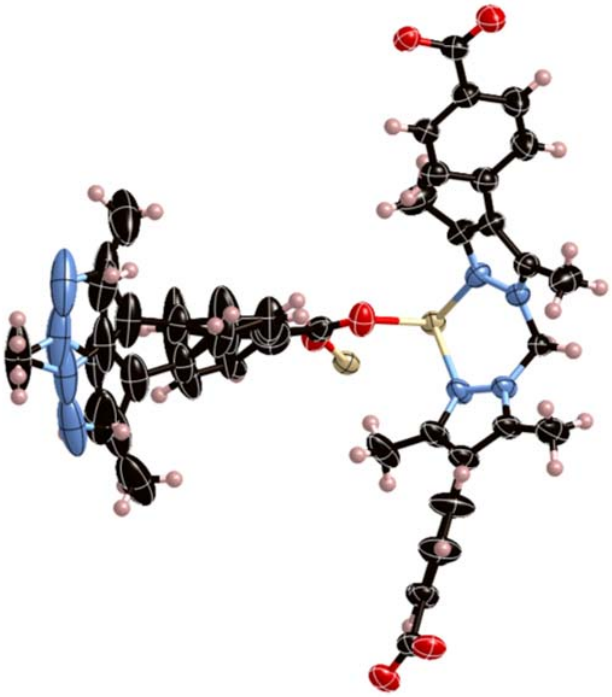

Figure S5.1. The asymmetric unit of **MnMOF-1-EtOH**, with all non-hydrogen atoms represented by ellipsoids at the 50% probability level (C, black; H, white; N, aqua; O, red; Rh, orange; Mn, beige).

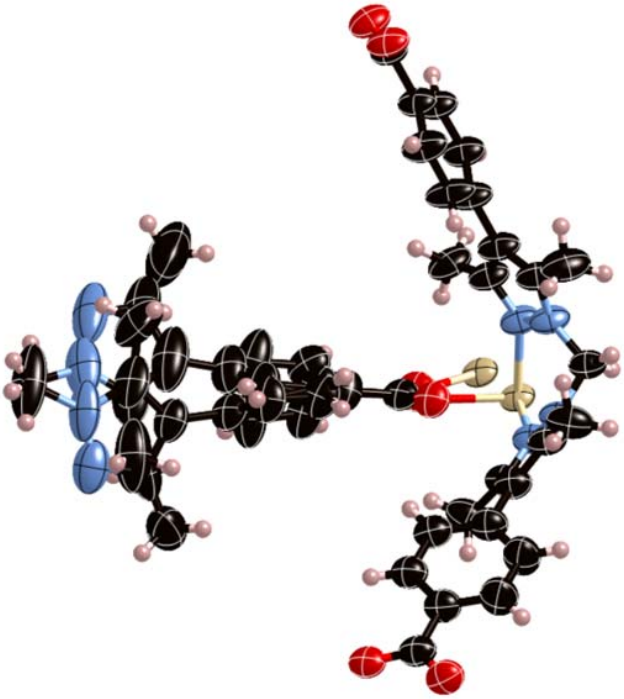

Figure S5.2. The asymmetric unit of **MnMOF-1-MeOH**, with all non-hydrogen atoms represented by ellipsoids at the 50% probability level (C, black; H, white; N, aqua; O, red; Rh, orange; Mn, beige).

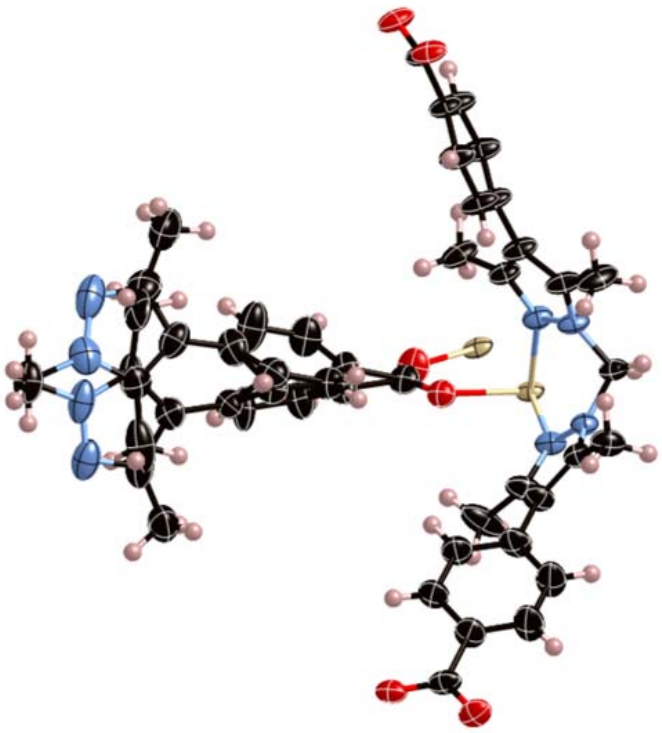

Figure S5.3. The asymmetric unit of **MnMOF-1-ace**, with all non-hydrogen atoms represented by ellipsoids at the 50% probability level (C, black; H, white; N, aqua; O, red; Rh, orange; Mn, beige).

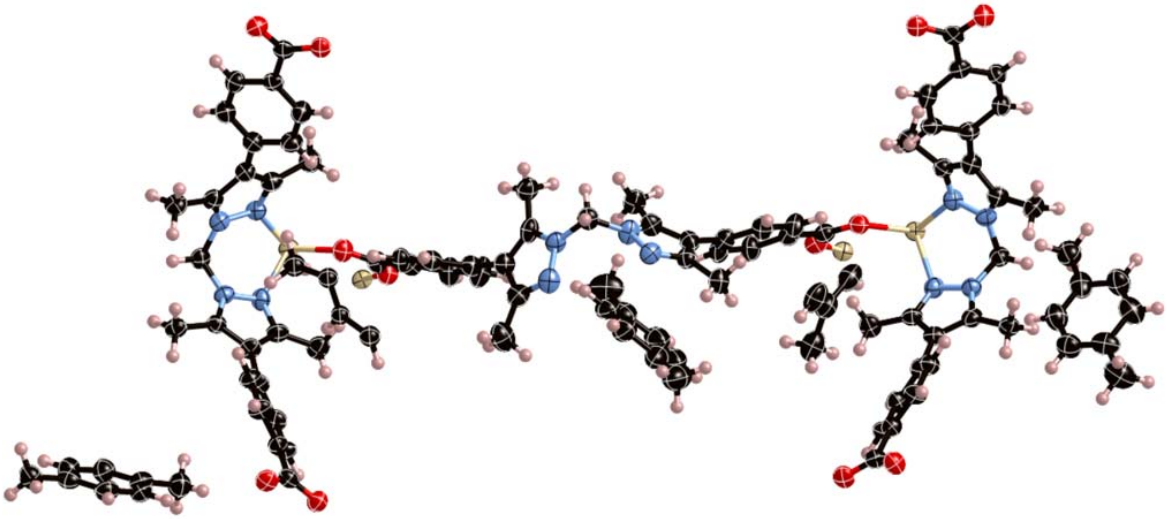

Figure S5.4. The asymmetric unit of **MnMOF-1-*p*-xylene**, with all non-hydrogen atoms represented by ellipsoids at the 50% probability level (C, black; H, white; N, aqua; O, red; Rh, orange; Mn, beige).

Figure S5.5. The asymmetric unit of **MnMOF-1-DEE**, with all non-hydrogen atoms represented by ellipsoids at the 50% probability level (C, black; H, white; N, aqua; O, red; Rh, orange; Mn, beige).

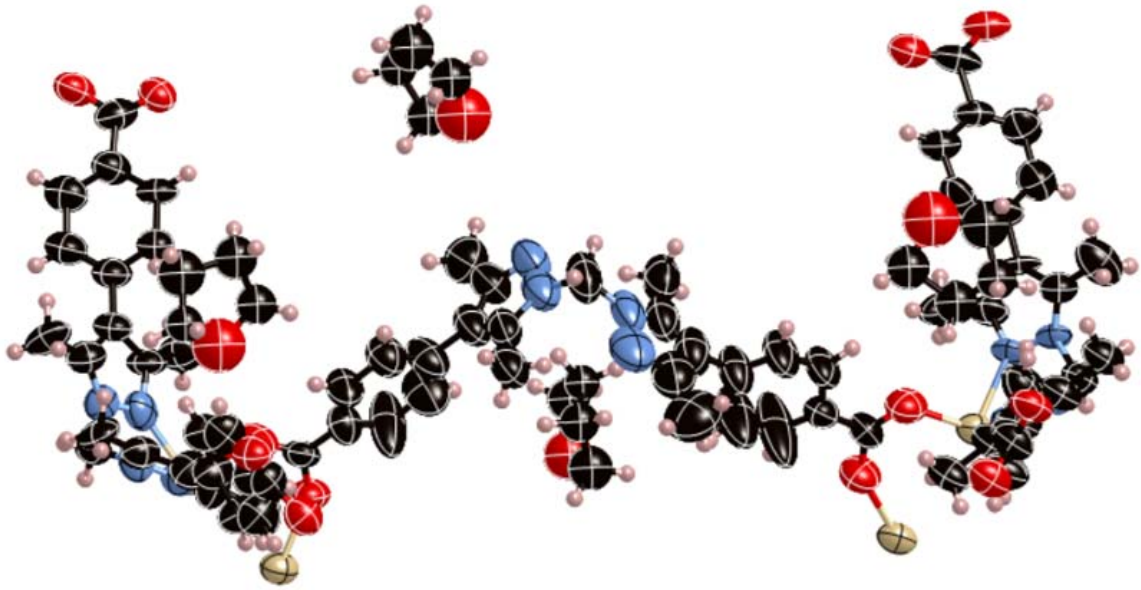

Figure S5.6. The asymmetric unit of **MnMOF-1-THF**, with all non-hydrogen atoms represented by ellipsoids at the 50% probability level (C, black; H, white; N, aqua; O, red; Rh, orange; Mn, beige).

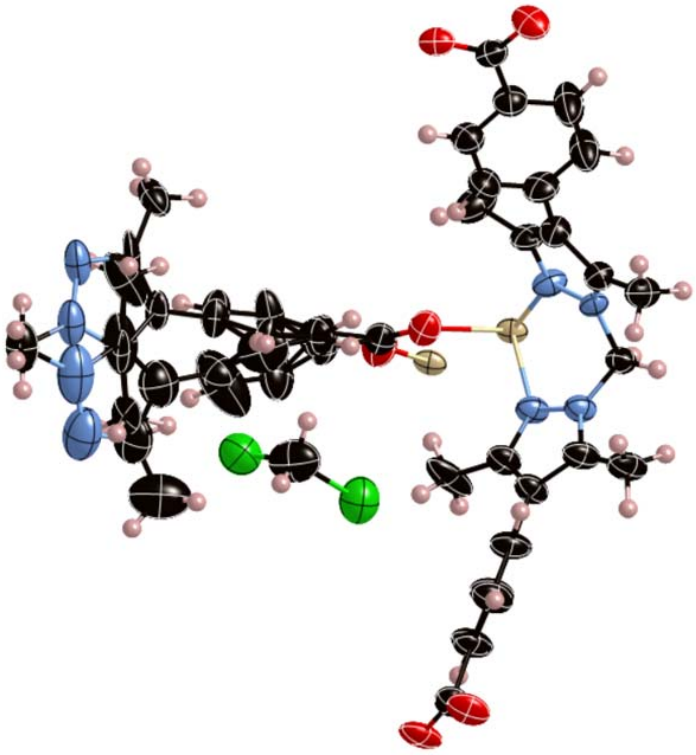

Figure S5.7. The asymmetric unit of **MnMOF-1-DCM**, with all non-hydrogen atoms represented by ellipsoids at the 50% probability level (C, black; H, white; N, aqua; O, red; Rh, orange; Mn, beige).

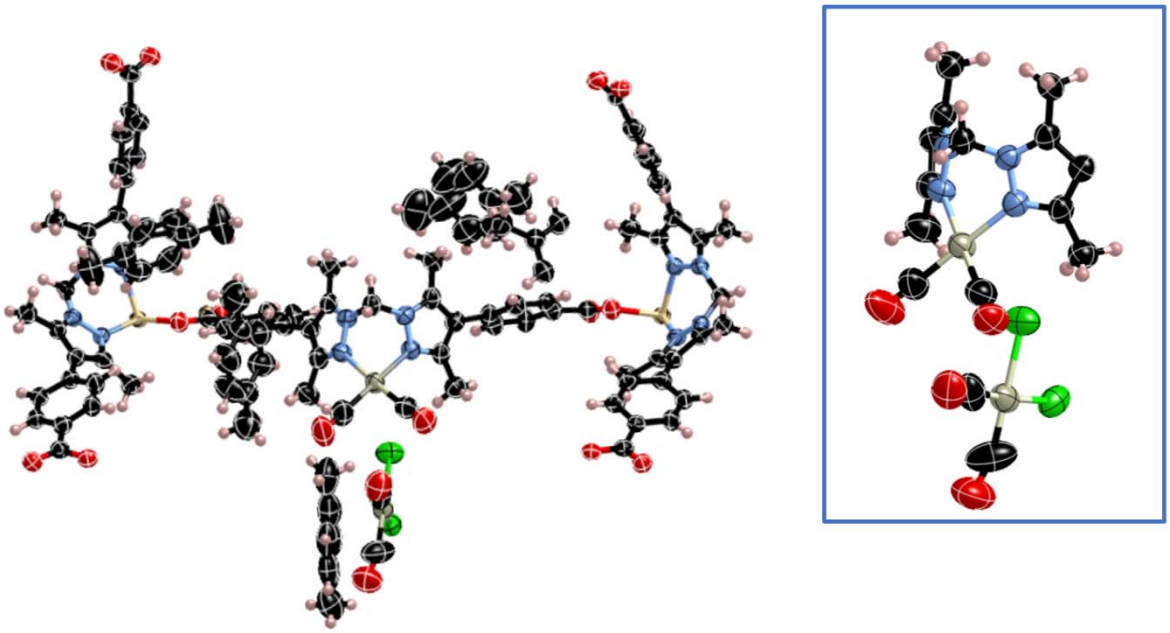

Figure S5.8. (Left) The asymmetric unit of **MnMOF-1**·$[Rh(CO)_2][Rh(CO)_2Cl_2]$, with all non-hydrogen atoms represented by ellipsoids at the 50% probability level (C, black; H, pink; N, aqua; O, red; Rh, orange; Mn, beige; Rh, white). (Right) A perspective view of the chelating site, displaying the coordinating sphere of the Rh(I) centre and its associated $[Rh(CO)_2Cl_2]$ anion.

SI 6.0 Energy Dispersive X-ray Analysis (EDX)

Table S6.1. Rh(I) occupancy determined for **MnMOF-1-solvent** after reaction with $[Rh(CO)_2Cl]_2$ in the same solvent. The Rh(I) occupancy was determined via measurement of the Mn:Rh ratio using EDX analysis. Given that there are three Mn centres per formula unit, 200% Rh content (to give a Mn:Rh ratio of 3:2) is required for **MnMOF-1**·$[Rh(CO)_2][Rh(CO)_2Cl_2]$ to have full metalation.

Sample	Rh occupancy (%)[a,b]	Std error (%)
MnMOF-1-ace	210	4.7
MnMOF-1-DCM	198	4.3
MnMOF-1-DEE	3	2.5
MnMOF-1-THF	5	1.5

[a] Average atomic% obtained from four crystals.
[b] Relative to full occupancy of the free chelation sites in **1**.

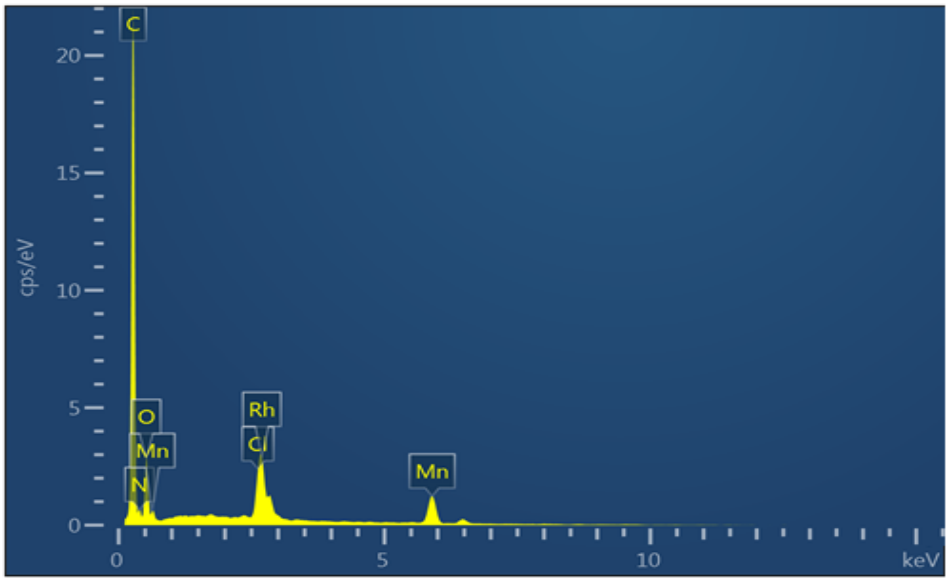

Figure S6.1. Representative raw EDX spectra for **MnMOF-1**·$[Rh(CO)_2][RhCl_2(CO)_2]$ in acetone

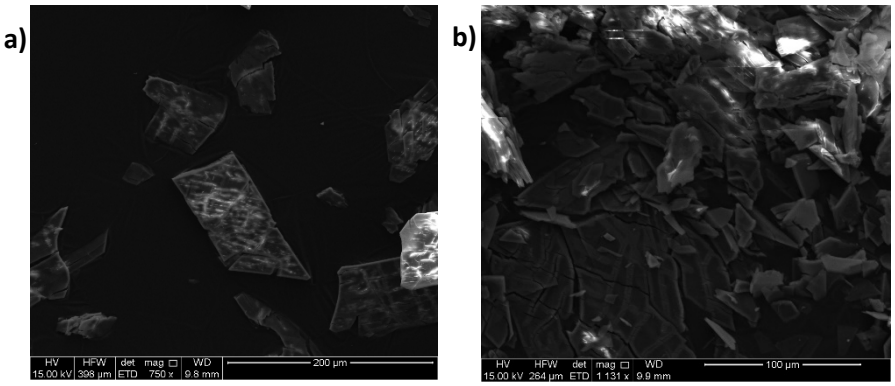

Figure S6.2. SEM images of **MnMOF-1**·$[Rh(CO)_2][RhCl_2(CO)_2]$ in acetone showing (a) an example of a single crystal (b) a group of crystals.